Thin Solid Films 711 (2020) 138299

Contents lists available at ScienceDirect

Thin Solid Films

journal homepage: www.elsevier.com/locate/tsf

The low-temperature remote-plasma-activated pulsed chemical vapor deposition route to SiN_x from 1,3,5-tri(isopropyl)cyclotrisilazane

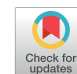

Barry Arkles[a,*], Chad Brick[a], Jonathan Goff[a], Alain E. Kaloyeros[b]

[a] Gelest Inc., 11 Steel Road East, Morrisville, PA 19067 U.S.A

[b] BFD Innovation, Slingerlands, New York 12159 U.S.A

ARTICLE INFO

Keywords:
Chemical vapor deposition
Silicon nitride
1,3,5-tri(isopropyl)cyclotrisilazane
Remote plasma

ABSTRACT

High-quality silicon nitride (SiN_x) thin films were grown by remote-plasma-activated pulsed chemical vapor deposition (P-CVD) from the source precursor 1,3,5-tri(isopropyl)cyclotrisilazane (TICZ, $C_9H_{27}N_3Si_3$) and remote ammonia (NH_3) plasma on silicon oxide (SiO_2) substrates within an optimized substrate temperature window ranging from 200 to 350 °C. TICZ was selected because of its chemical stability, non-pyrophoric nature, good vapor pressure (~127 Pa at 70 °C), and its chemical structure that incorporates alkyl groups with three C atoms on each N atom, which provides a clean elimination mechanism for low temperature SiN_x deposition. P-CVD consisted of a four-step process: TICZ pulse with no plasma, N_2 purge, NH_3 plasma pulse, and N_2 purge. The as-deposited films were analyzed using spectroscopic ellipsometry and x-ray photoelectron spectroscopy (XPS). Wet etch rates were determined using a standard solution consisting of 0.5% hydrofluoric acid in deionized water. XPS analysis revealed a Si:N ratio of ~1:1 within the entire substrate temperature range and validated the formation of the SiN_x phase. In situ, real-time ellipsometry measurements confirmed that SiN_x growth exhibited a non-self-limiting P-CVD behavior. They also yielded an as-grown SiN_x average refractive index of ~1.8 for the films grown at substrate temperatures above 200 °C.

1. Introduction

Research, development, and manufacturing interests in silicon nitride (SiN_x) is at an unprecedented high [1–3] driven not only by the need to extend its historical applicability in the constantly evolving integrated circuitry (IC) and solar cell industries, but also by its potential use in myriad of next-generation applications. The latter include: host matrices for Si nanocrystals and quantum dots for photoluminescence applications [4,5] waveguides in nonlinear frequency combs for sensors and photonic devices for telecommunications [6] tunable luminescent films for Si-based light emitting diodes in Si-based monolithic optoelectronic integration;[7] passivation/encapsulation nanostructures at the gallium arsenide interface for compound semiconductor devices;[8] and base platforms for integration with biological materials in biochemistry and medical applications [9,10].

The tremendous appeal of SiN_x derives from its highly attractive mix of physical, chemical, mechanical, electrical, and optoelectronic properties, which make it one of the most commonly used materials across a diversified array of industries [1,3]. Many of these industries share the same evolutionary drivers in terms of migration towards the incorporation of heterodevice structures with smaller feature sizes using thermally and/or chemically sensitive substrates [11–15] As a result, research and development (R&D) activities have focused on the development and optimization of low-temperature deposition processes, such as direct and remote plasma-enhanced chemical vapor deposition (PE-CVD) [16–18], laser-assisted CVD [19], mirror-plasma enhanced CVD [20], multiple-holes hollow-cathode radio-frequency PECVD [15], and direct, remote, and glow-discharge plasma-enhanced atomic layer deposition [8,14,21].

In spite of these extensive R&D efforts, however, significant challenges remain to be overcome in order to extend SiN_x to heterodevice applications. For one, the vast majority of PE-CVD and PE-ALD SiN_x processes rely on the reaction of silane (SiH_4) and silane-type precursors with ammonia (NH_3). The inherent issues associated with using such chemistries are well documented and include their pyrophoric nature, increased thermal budget, and the incorporation of high levels of hydrogen (H). In addition, PE-ALD processes using silane-type Si sources suffer from substrate surface adsorption and nucleation problems, thus requiring substrate surface pre-treatment, which adds complexity and cost [8,20–23]. Furthermore, the resulting films frequently consist of varying concentrations of Si and N, with the inclusion of significant levels of C and O and/or the presence of Si to N

* Corresponding author.
E-mail address: akaloyeros@gmail.com (B. Arkles).

https://doi.org/10.1016/j.tsf.2020.138299
Received 4 June 2020; Received in revised form 19 August 2020; Accepted 19 August 2020
Available online 20 August 2020
0040-6090/ © 2020 The Authors. Published by Elsevier B.V. This is an open access article under the CC BY-NC-ND license
(http://creativecommons.org/licenses/BY-NC-ND/4.0/).

compositional gradients between the interfacial, bulk and surface regions of the film [7,24].

For these reasons, our recent work has focused on the study of a different class of Si source precursors, namely, N-alkyl substituted perhydridocyclotrisilazanes. Unlike known perhydridocyclic silazanes with methyl groups on the N atoms, this class of silazanes contains alkyl radicals with at least two carbon atoms on each N atom, providing a mechanism for low temperature SiN_x deposition by elimination of the alkyl substitutions [25]. While not expected to occur quite so cleanly in practice, the following depicts the conceptual conversion of triisopropylcyclotrisilazane to cyclotrisilazane with loss of propylene:

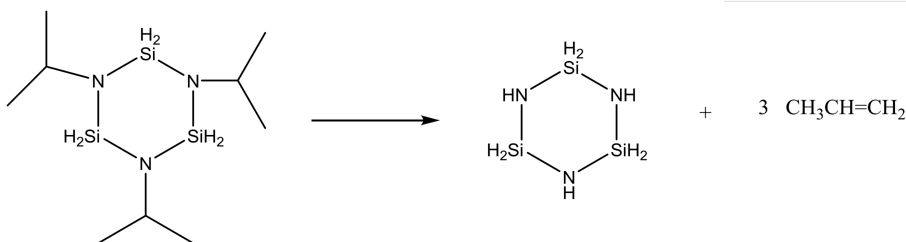

In contrast, the simple methyl groups require higher temperatures for film formation and incorporate significantly higher C concentration into the resulting films [26], presumably due to their lack of a low-energy elimination mechanism.

This report focuses on the development and optimization of a remote-plasma-activated pulsed CVD (P-CVD) process from one such perhydridocyclotrisilazane—1,3,5-tri(isopropyl)cyclotrisilazane (TICZ, $C_9H_{27}N_3Si_3$)—which exhibits three C atoms on each N in the form of a propyl group. The latter is easily eliminated at moderate temperatures in the form of the gaseous byproduct propylene. The compositional and optical properties of the resulting films were analyzed by in-situ, real-time, spectroscopic ellipsometry as well as x-ray photoelectron spectroscopy (XPS), and their wet etch rates were determined using a standard IC industry etch solution. The results are summarized and discussed below.

2. Experimental conditions

2.1. Precursor synthesis

Under an argon atmosphere, a 5-liter 4-necked flask equipped with a cooling bath, overhead stirrer, pot thermometer, sub-surface dip-tube, and dry-ice condenser was charged with 909 gs of methyl t-butyl ether. The mixture was cooled to −40 °C, and 303.0 gs (3 mol) of dichlorosilane was slowly added to the pot. 364.7 gs (6.0 mol) of isopropylamine was then added via dip-tube at temperatures in the range of −30 to −20 °C over a period of 2.5 h. After the addition was completed, the reaction mixture was slowly warmed up to 25 °C and stirred at this temperature for 8 to 14 h. Stirring was followed by the addition of 177.4 g (3 mol) of isopropylamine at temperatures in the range of 0 to 40 °C, and the subsequent addition of another 227.3 gs of methyl t-butyl ether. The mixture was stirred again for 6 to 16 h, during which time it was and monitored by gas chromatography. The reaction solution was then filtered and solvents were removed from the filtrates under reduced pressure (below 50 °C). The filtering process was repeated, with fractional distillation of the clear filtrates yielding 64.5 g (24.66) of TICZ.

TICZ vapor pressure was determined using a combination of distillation temperature, pressure readings (< 1330 Pa), and pressure-cell DSC measurements (>1330 Pa). The latter employed a TA Instruments Pressure differential scanning calorimetry (DSC) 25P instrument with Tzero Hermetic Pinhole (75 µm) Lids, 2–5 mg sample size, and a 15 °C/min ramp rate. Fig. 1 displays actual vapor pressure data from distillation and DSC measurements, as well as Antoine Equation's fit [Log (P) = A–B/(C + T)] over the range of ~18 to ~1.01×10^5 Pa.

2.2. P-CVD processing conditions

A Picosun R-200 R&D system equipped with a sample load-lock to maintain the cleanliness and vacuum integrity of the reaction chamber and a remote inductively-coupled plasma (ICP) power source was employed for P-CVD process development and optimization. All depositions were performed on substrates consisting of 1000 nm silicon dioxide thermally grown on n-doped Si wafers, acquired from Addison Engineering. The samples were loaded as-received and were subjected to an in-situ NH_3plasma clean at a plasma frequency of 13.56 MHz and a plasma power of 2000 W for five minutes before each deposition run.

The TICZ precursor was loaded in a specialized bubbler which was connected to the Picosun precursor manifold system and heated to 50 °C. All delivery lines were also heated to 90 °C to inhibit premature precursor condensation prior to entering the reaction chamber. N_2 gas was used as carrier gas and set at 100 sccm.

Process development and optimization for P-CVD $SiN_x$from the reaction of TICZ and remote NH_3 plasma was carried out in two phases. In a first "proof-of-concept" phase, a systematic set of screening experiments were conducted to identify optimum values for the duration of the TICZ pulse, purge step, and NH_3 plasma pulse, as well as N_2 purge gas flow rate, NH_3 remote plasma flow rate, and plasma power. In a second "process optimization" phase, the key experimental parameters were set as shown in Fig. 2 and the substrate temperature was varied from 50 °C to 350 °C in 50 °C intervals. NH_3 remote plasma frequency, flow rate, and power were set at 13.56 MHz, 40 sccm, and 2000 W, respectively. Samples were subsequently transferred to the load lock system and allowed to cool to room temperature in a N_2 atmosphere prior to removal from the Picosun system.

For XPS analysis, the SiN_xsamples were capped with an approximately 10–15 nm-thick zinc oxide (ZnO_x) layer to prevent contamination during transport and handling. The ALD ZnO_x process employed 100 cycles of the reaction of diethyl zinc (DEZ) as the Zn source and water as the oxygen source. ZnO_x was grown in-situ immediately following the SiN_x deposition and at the same temperature, except in the case of the 50°C sample, for which the temperature was increased to 150 °C for the ZnO_x deposition. The process consisted of four-steps: 0.1 s DEZ pulse, 5 s N_2 purge, 0.1 s water vapor pulse, 5 s N_2 purge

2.3. Analytical techniques

In-situ, real-time, angle-resolved ellipsometry was performed using a Woollam iSE ellipsometer at wavelengths ranging from 400 to 1000 nm. The ellipsometer system was mounted directly on the P-CVD reaction chamber, with the incident light beam being directed onto the substrate through a quartz glass window at an incident angle of 60.8°,

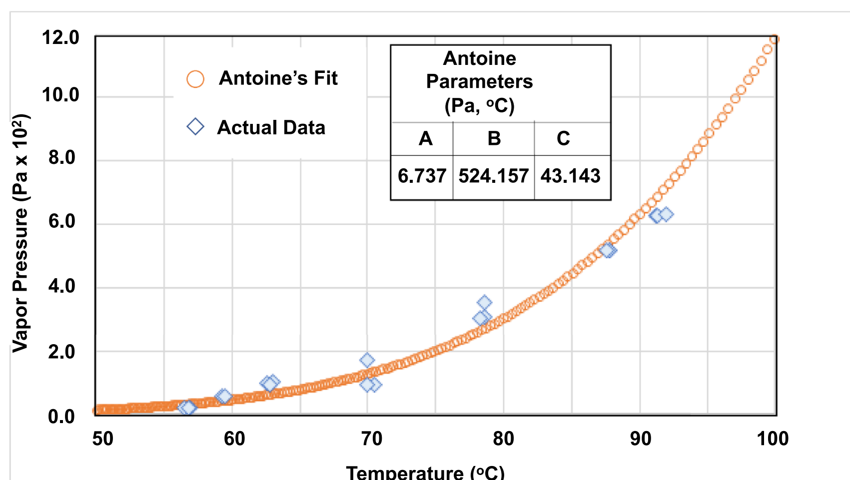

Fig. 1. TICZ experimental vapor pressure data and Antoine Equation's fit over the range of ~18 to ~1.01 × 10^5 Pa.

and the reflected light beam being captured by a detector. The resulting data was analyzed using CompleteEASE software. The substrate was modelled as a ~1000 nm thermal SiO_2 layer on Si. The thickness of the SiO_2 layer was measured in-situ prior to every P-CVD run.

XPS was carried out at Eurofins EAG Materials Science, LLC on a PHI Quantum 2000 system. X-rays were generated from a monochromated Al k_α source at 1486.6 eV and directed at the sample at $a \pm 23°$ acceptance angle and 45° take-off angle. In-depth compositional analysis was performed with an Ar^+ ion gun at 2 keV, 4mm × 2 mm raster, and 3.8 nm/min sputter rate. Since the Si, N, C, and O peaks were well separated from each other, no deconvolution was applied to the data. All data processing (integration) was performed using CasaXPS software from Casa Software Ltd. Montage plots were generated using MultiPak software, produced by Ulvac-phi, Inc. Depth profile plots were produced using Microcal Origin, manufactured by Microcal Software, Inc. High-resolution XPS peak assignments were performed following the calibration procedure described in ISO 15,472:2010 "Surface chemical analysis – X-ray photoelectron spectrometers – Calibration of energy scales.

Wet etch rate studies were conducted using an IC industry standard solution consisting of 0.5% hydrofluoric acid (HF) in deionized water at room temperature.

Table 1
Chemical structure and pertinent properties of TICZ.

Property	Value
Chemical Structure	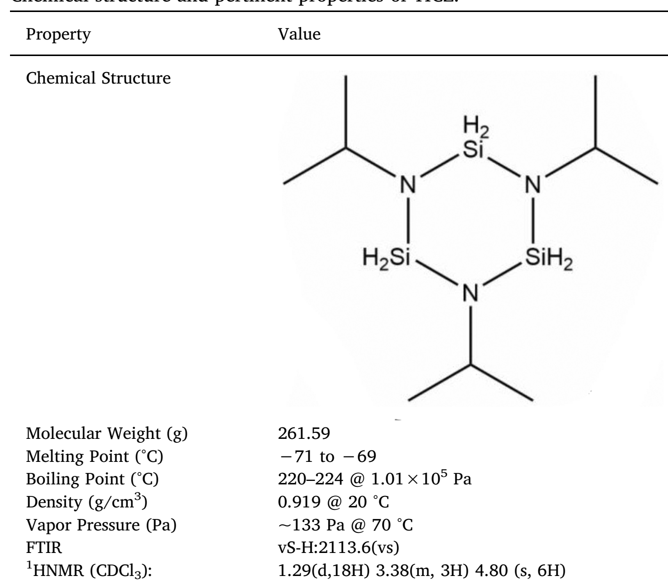
Molecular Weight (g)	261.59
Melting Point (°C)	−71 to −69
Boiling Point (°C)	220–224 @ 1.01 × 10^5 Pa
Density (g/cm^3)	0.919 @ 20 °C
Vapor Pressure (Pa)	~133 Pa @ 70 °C
FTIR	vS-H:2113.6(vs)
^{1}HNMR ($CDCl_3$):	1.29(d,18H) 3.38(m, 3H) 4.80 (s, 6H)

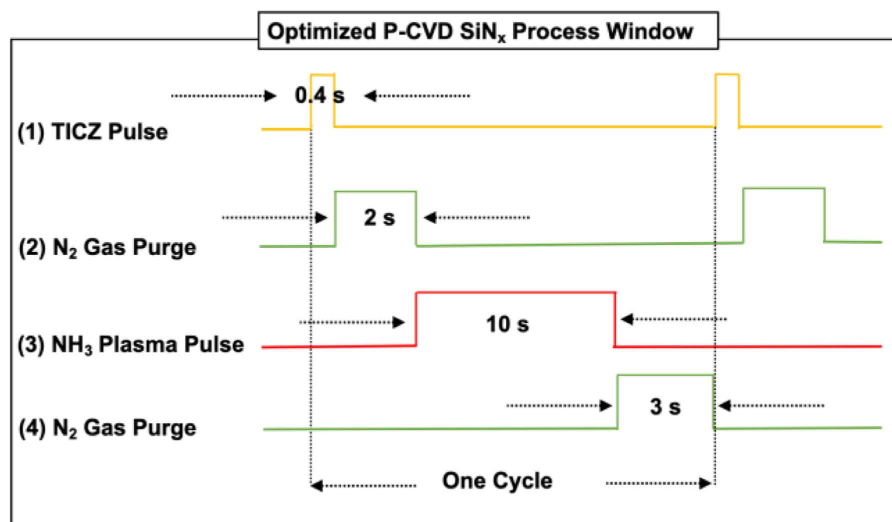

Fig. 2. Optimized pulsed CVD SiN_x process window. Pulse durations and purge times were identical for substrate temperatures of 50, 150, 200, 250, 300, and 350 °C, except no precursor purge time was applied in the 350 °C run.

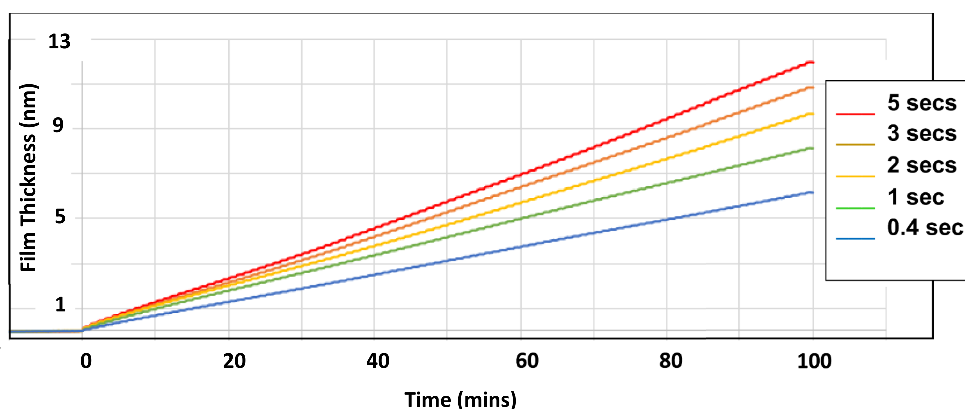

Fig. 3. In-situ, real-time, ellipsometry measurements of film thickness versus number of cycles for substrate temperature of 200 °C for TICZ pulse times of 0.4 s, 1.0 s, 2.0 s, 3.0 s, and 5.0 s.

3. Results and discussion

3.1. Precursor selection

One additional motivation selecting of 1,3,5-tri(isopropyl)cyclotrisilazane (TICZ, $C_9H_{27}N_3Si_3$) is that it can be generated at high yield and purity from readily available starting materials, as outlined in the precursor synthesis section above. This ensures its suitability for high volume manufacturing. Pertinent properties of TICZ are displayed in Table 1 while its vapor pressure versus temperature parameters are shown in Fig. 1. It should be noted that the precursor synthesis recipe described earlier can also produce other analogs, for example 1,3,5-tri(ethyl)cyclotrisilazane and 1,3,5-tri(t-butyl)cyclotrisilazane. which have different volatility and deposition characteristics.

3.2. Ellipsometry analysis

Fig. 3 exhibits in-situ, real-time ellipsometry profiles of film thickness versus deposition duration for films grown at 200 °C substrate temperature for TICZ pulse times of 0.4 s, 1.0 s, 2.0 secs, 3.0 s, and 5.0 s. As seen in the profiles, film thickness continues to increase with precursor pulse time and does not saturate, regardless of precursor pulse time. This behavior indicates that the TICZ adsorption step is not self-limiting and supports the assertion that the growth of SiN_x films occurs through a pulsed CVD instead of an ALD process. The same film thickness dependence on pulse time was observed for selected substrate temperatures of 150, 200, and 300 °C, indicating that film formation occurs through a P-CVD growth mode within this process window.

Similarly, Figs. 4 and 5 display plots of in-situ, real-time, ellipsometry measurements of film thickness versus deposition time for substrate temperatures of 150, 175, 200, 225, 300, and 350 °C. As expected, film thickness increases with longer deposition time (Fig. 4). However, a gradual decrease in the slope of each film thickness curve is also observed with higher substrate temperature, indicating a reduction in growth rate per cycle (GPC) with rising substrate temperature. This decline in GPC can be attributed to a reduction in precursor partial vapor pressure in the reaction zone in proximity to the substrate. This reduction may result from the geometry of the deposition chamber, which induces additional heating at the point of precursor entry into the reactor as substrate temperature increases, leading to some precursor decomposition prior to reaching the reaction zone. Alternatively, the reduction could be caused by a higher frequency of recombination between precursor species and associated ligands with the rise in thermal budget, and their subsequent desorption from the substrate surface, thereby restricting the TICZ and NH_3 reaction rate.

Furthermore, in-situ, real-time ellipsometry measurements of film thickness versus deposition time for the first minute of the P-CVD SiN_x process (Fig. 5) shows that film formation occurs instantaneously in the first P-CVD cycle. Film nucleation and growth takes place without the manifestation of an incubation period or delay in film nucleation and growth, in contrast to a number of prior reports in the literature for ALD and CVD SiN_x [1,3]. This feature is important as it removes the requirement for substrate surface pre-treatments, thus eliminating added complexity and cost in the incorporation of P-CVD SiN_x in heterodevice structure manufacturing process flows. In addition, Table 2 presents ellipsometry-derived values for film thickness, GPC, and index of refraction for as-deposited SiN_x films as a function of substrate temperature. Selected film thicknesses were also confirmed by XPS depth profile analyses.

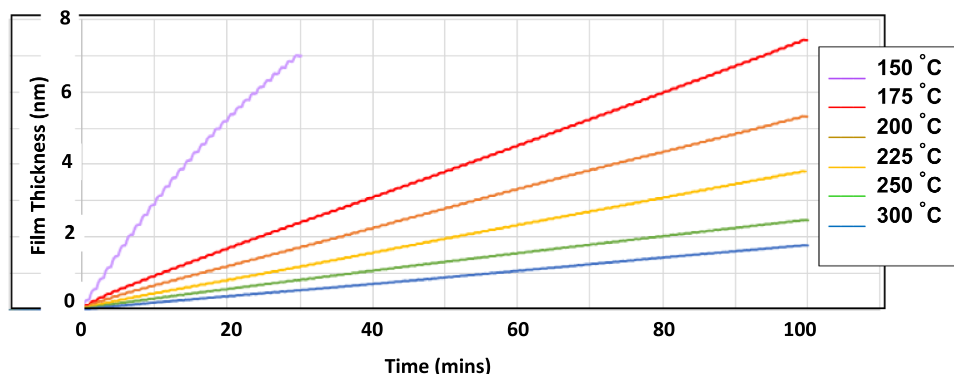

Fig. 4. In-situ, real-time, ellipsometry measurements of film thickness versus number of cycles for substrate temperatures of 150, 175, 200, 225, 300, and 350 °C. The pulse durations were 0.4 s, 2 s, 10 s, and 3 s for the TICZ pulse, N^2 purge, NH^3 plasma pulse, and N^2 purge, respectively.

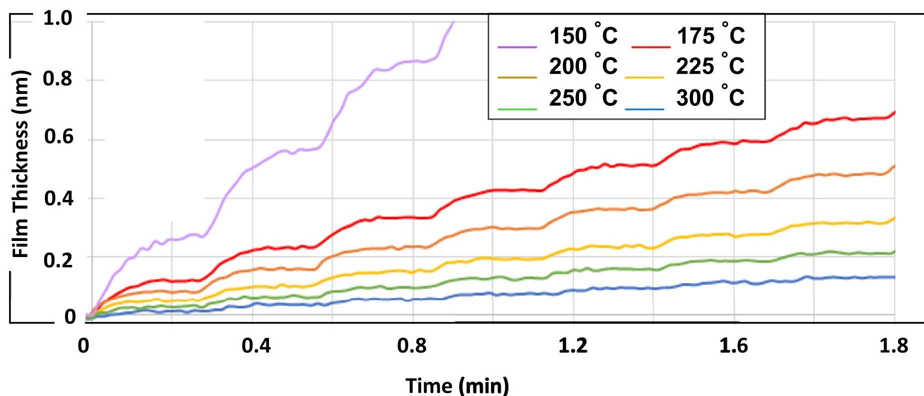

Fig. 5. In-situ, real-time, ellipsometry measurements of film thickness versus deposition time for the first minute of P-CVD SiN_x processing. The pulse durations were 0.4 s, 2 s, 10 s, and 3 s for the TICZ pulse, N_2 purge, NH_3 plasma pulse, and N_2 purge, respectively. .

Table 2
Selected properties of P-CVD SiN_x, as determined by ellipsometry, XPS, and wet etching.

Substrate Temperature (°C)	Film Thickness (nm)	Growth Rate (nm/cycle)	Etch Rate (nm/min)	Refractive* Index
50	2948	0.590	2310	1.491
150	289	0.234	732	1.513
200	87.3	0.053	99	1.800
250	102	0.025	25	1.813
300	104	0.018	12	1.807
350	58.5	0.019	2.4	1.815

*Measurements performed at room temperature ± 2°C.

3.3. XPS analysis

Zn, Si, N, C, and O concentrations versus penetration depth were assessed in SiN_x films by XPS depth profile analyses, as shown in Figs. 6(a) and 6(b) for as-deposited SiN_x films grown at substrate temperatures of 200 and 300 °C, respectively.

The measurements revealed decreasing C concentrations of ~42 at% and ~15 at% for films grown at 50 °C and 150 °C substrate temperatures, respectively. The value declined to below XPS detection limits above 200 °C substrate temperature, as shown in Fig. 6(a). The XPS results therefore indicate that 200 °C provides the minimum thermal budget required for efficient reaction of TICZ and NH_3, leading to complete precursor dissociation, and removal of reaction byproducts from the deposition zone. Similarly, O concentrations of ~11 at% and ~6 at% were recorded for films grown at 50 °C and 150 °C substrate temperatures, respectively. The value declined to ~5 at% above 200 °C substrate temperature, as shown in Fig. 6(a). Oxygen inclusion is attributed to O diffusion during the in-situ P-CVD zinc oxide (ZNO_x) capping layer deposition step or O impurities in the carrier gas streams, and/or plasma etching of the Al_2O_3 dielectric liners used to contain the plasma in the ICP plasma source [27,28].

Table 3
Representative P-CVD SiN_x atomic concentrations (in at%) within the bulk of films grown at 200, 250, and 300 °C.

Substrate Temperature (°C)	Depth in Sample (nm)	C	N	O	Si
200	~25	~0.7	~47.5	~3.2	~48.5
250	~25	~0.2	~46.9	~5.4	~47.5
300	~25	~0.0	~47.2	~5.6	~47.3

Additionally, Table 3 gives representative P-CVD SiN_x atomic concentrations within the bulk of films grown at 200, 250, and 300 °C, at a

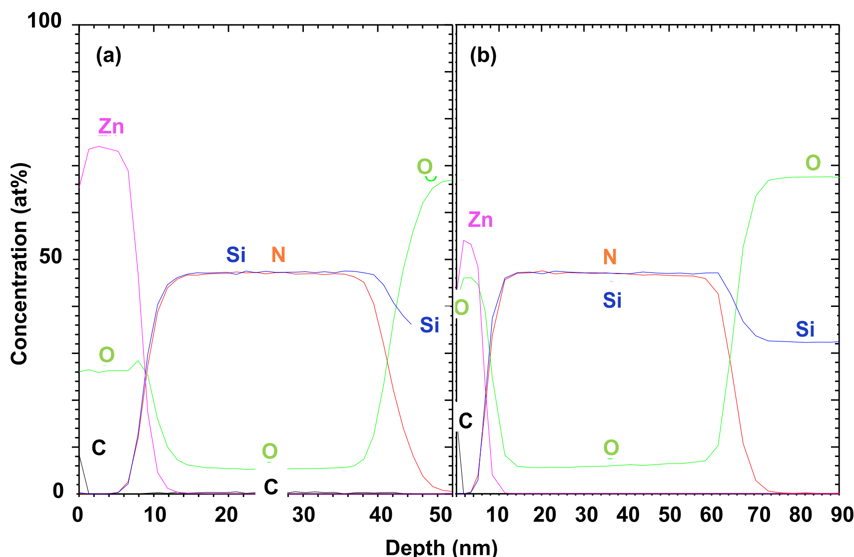

Fig. 6. XPS profile of Zn, Si, N, C, and O concentrations versus penetration depth in SiN_x for films deposited at: (a) 200 °C and (b) 300 °C.

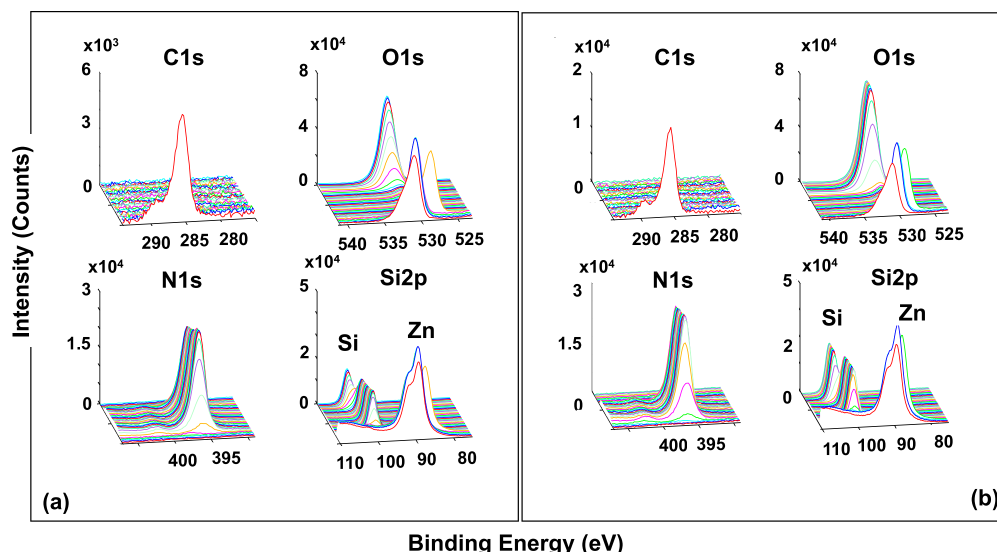

Fig. 7. High-resolution XPS spectra for Si2p, N1s, C1s, and O1s binding energies versus penetration depth in SiN_x for films deposited at: (a) 200 °C and (b) 300 °C.

depth of ~25 nm. Along with Figs. 6(a) and 6(b), the values in this table demonstrate that samples deposited above 200 °C consisted of Si:N in a ratio of ~1:1.

Additionally, high-resolution XPS spectra for Si 2p, N 1 s, C 1 s, and O 1 s binding energies versus penetration depth are displayed in Figs. 7(a) and 7(b) for SiN_x films deposited at 200 °C and 300 °C, respectively. The data demonstrates that both sets of films consisted of a SiN phase with a low O concentration and practically no C inclusion. It should be noted that the N 1 s spectra contained a main peak attributed to $N(\text{-Si})_3$, which is due to Si-N bonding, nitride and a minor peak attributed to $O{-}N(\text{-Si})_2$, which is associated with silicon oxynitride ($Si_xN_yO_z$).

3.4. Wet etch rate

Wet etch studies were conducted using an IC industry standard solution consisting of 0.5% hydrofluoric acid (HF) in deionized water. The results are presented in Table 2. The wet etch rates (WERs) observed for films deposited at 300 °C are competitive with those reported in the literature including, for example, for low-pressure CVD films grown at 770 °C and PE-ALD films deposited at 250 °C etched in a milder etch solution consisting of 1:300 HF:H_2O solution [29]; and PE-ALD films grown between 270 and 350 °C and treated in a more diluted wet etch solution consisting of 1:500 HF:H_2O [30].

4. Conclusions

This report summarizes key findings from the development and optimization of a low-temperature P-CVD SiN_x films using the reaction of the source precursor 1,3,5-tri(isopropyl)cyclotrisilazane (TICZ, $C_9H_{27}N_3Si_3$) with remote NH_3 plasma. TICZ was selected because it exhibits three C atoms on each N in the form of a propyl groups, which are easily eliminated at moderate temperatures in the form of the gaseous byproduct propylene. TICZ is also generated at high yield and purity from readily available starting materials, as outlined in the precursor synthesis section presented earlier, thus demonstrating its suitability for high volume manufacturing. The research presented here led to the identification of an optimized substrate temperature window ranging from 200 to 350 °C for the formation of high-quality $Si_{1.0}$:$N_{1.0}$ films. Wet etch studies in a standard IC industry solution consisting of 0.5% HF in deionized H_2O produced viable WERs that are competitive with those reported in the literature. In contrast to a number of prior reports in the literature for ALD and CVD SiN_x, ellipsometry analyses of film nucleation and growth characteristics showed that film formation occurs instantaneously in the first P-CVD cycle without an incubation period, eliminating the need for substrate surface pre-treatments that result in additional complexity and added cost of ownership. These results demonstrate that P-CVD SiN_x using TICZ as Si source precursor is a viable option for incorporation into emerging heterodevice structures manufacturing process flows.

5. Credit author statement

All authors contributed to this work. BA and AK conceptualized and supervised the project. BA and JG directed chemical aspects of the project. AK and CB directed the applied physics aspects of the project. BA, AK, and JG wrote the MS. All authors contributed content and reviewed the manuscript.

Declaration of Competing Interest

The authors declare that they have no known competing financial interests or personal relationships that could have appeared to influence the work reported in this paper, other than their explicit affiliation with their employers.

Acknowledgement

The authors would like to thank Eurofins EAG Materials Science, LLC for providing the XPS sample analysis discussed in this article.

References

[1] A.E. Kaloyeros, F.A. Jové, J. Goff, B. Arkles, Silicon nitride and silicon nitride-rich thin film technologies: trends in deposition techniques and related applications, ECS J. Solid State Sci. Technol 6 (2017) 691–714, https://doi.org/10.1149/2.0011710jss.
[2] X. Meng, Y.C. Byun, H.S. Kim, J.S. Lee, A.T. Lucero, L. Cheng, J. Kim, Atomic layer deposition of silicon nitride thin films: a review of recent progress, challenges, and outlooks, Materials (Basel) 9 (2016), https://doi.org/10.3390/ma9121007.
[3] A.E. Kaloyeros, J.D. Goff, Y. Pan, B. Arkles, Silicon nitride and silicon nitride-rich thin film technologies: state-of-the-art processing technologies, properties, and applications, ECS J. Solid State Sci. Technol 9 (2020) 063006–063058, https://doi.org/10.1149/2162-8777/aba447.
[4] T. Torchynska, L. Khomenkova, A. Slaoui, Modification of light emission in si-rich silicon nitride films versus stoichiometry and excitation light energy, J. Electron. Mater. 47 (2018) 3927–3933, https://doi.org/10.1007/s11664-018-6271-0.
[5] S. Meziani, A. Moussi, L. Mahiou, F. Antoni, R. Outemzabet, Rapid thermal process for crystallization silicon nitride films, Surf. Eng 36 (2020) 456–464, https://doi.org/10.1080/02670844.2018.1564199.

[6] R. Kou, N. Yamamoto, G. Fujii, T. Aihara, T. Tsuchizawa, A. Ishizawa, K. Hitachi, H. Gotoh, M. Ukibe, K. Yamada, Spectrometric analysis of silicon nitride films deposited by low-temperature liquid-source CVD, J. Appl. Phys. 126 (2019) 133101, , https://doi.org/10.1063/1.5114675.

[7] P. Zhang, L. Zhang, Y. Wu, S. Wang, X. Ge, High photoluminescence quantum yields generated from N-Si-O bonding states in amorphous silicon oxynitride films, Opt. Express 26 (2018) 31617, https://doi.org/10.1364/oe.26.031617.

[8] Y.K. Ezhovskii, S.V. M.ikhailovskii, Atomic layer deposition of silicon nitride films on gallium arsenide using a glow discharge, Russ. Microelectron 48 (2019) 229–235, https://doi.org/10.1134/S1063739719030041.

[9] T. Nagatsuka, H. Uzawa, D. Tanaka, Y. Oba, Y. Nishida, T. Iwasa, K. ichi Tayama, T. Yoshida, T. Ezaki, Y. Seto, Preparation of silicon nitride biochips for reflectometric interference spectroscopic (RIfS) analysis of biological toxins and E. coli O157:H7 strain, Sensors Actuators, B Chem 246 (2017) 937–942, https://doi.org/10.1016/j.snb.2017.02.136.

[10] B. Yin, W. Xie, L. Liang, Y. Deng, S. He, F. He, D. Zhou, C. Tlili, D. Wang, Covalent modification of silicon nitride Nanopore by amphoteric polylysine for short DNA detection, ACS Omega 2 (2017) 7127–7135, https://doi.org/10.1021/acsomega.7b01245.

[11] A.E. Kaloyeros, J.D. Goff, B. Arkles, Emerging molecular and atomic level techniques for nanoscale applications, Electrochem. Soc. Interface 27 (2018) 59–63.

[12] A.E. Kaloyeros, Y. Pan, J. Goff, B. Arkles, Cobalt Thin Films, Trends in processing technologies and emerging applications, ECS J. Solid State Sci. Technol 8 (2019) P119–P152, https://doi.org/10.1149/2.0051902jss.

[13] C. Brick, J.D. Goff, A.E. Kaloyeros, B. Arkles, Area-specific Atomic Layer Deposition (ALD) of cobalt as mediated by thermally induced dehydrocoupled Self-Assembled Monolayers (SAMs), in: ALD/ALE 2019, Bellevue, WA, USA, 2019: p. AS–TuP3.

[14] T.Y. Cho, W.J. Lee, S.J. Lee, J.H. Lee, J. Ryu, S.K. Cho, S.H. Choa, Moisture barrier and bending properties of silicon nitride films prepared by roll-to-roll plasma enhanced chemical vapor deposition, Thin Solid Films 660 (2018) 101–107, https://doi.org/10.1016/j.tsf.2018.06.003.

[15] B.B. Sahu, S.H. Kim, J.S. Lee, J.G. Han, Comparison of plasma properties in normal and multiple holes hollow cathode RF PECVD and their utility in a-SiNx:H thin film deposition, Vacuum 160 (2019) 316–324, https://doi.org/10.1016/j.vacuum.2018.11.034.

[16] P. Wang, S. Jin, T. Lu, C. Cui, D. Yang, X. Yu, Negatively charged silicon nitride films for improved p-type silicon surface passivation by low-temperature rapid thermal annealing, J. Phys. D. Appl. Phys. 52 (2019) 345102, , https://doi.org/10.1088/1361-6463/ab2ab9.

[17] Y.Y. Kim, Thermal property evaluation of a silicon nitride thin-film using the dual-wavelength pump-probe technique, Korean J. Mater. Res 29 (2019) 547–552, https://doi.org/10.3740/mrsk.2019.29.9.547.

[18] Lim,, Ultrahigh index and low-loss silicon rich nitride thin film for NIR HAMR optics, IEEE Trans. Magn (2017) 53.

[19] S. Kuk, H.K. Nam, Z. Wang, D.J. Hwang, Effect of laser beam dimension on laser-assisted chemical vapor deposition of silicon nitride thin films, J. Nanosci. Nanotechnol. 18 (2018) 7085–7089, https://doi.org/10.1166/jnn.2018.15727.

[20] T. Goto, S. Kobayashi, Y. Yabuta, S. Sugawa, Evaluation of silicon nitride film formed using magnetic-mirror confined plasma source, ECS J. Solid State Sci. Technol 8 (2019) N113–N118, https://doi.org/10.1149/2.0121908jss.

[21] R.A. Ovanesyan, E.A. Filatova, S.D. Elliott, D.M. Hausmann, D.C. Smith, S. Agarwal, Atomic layer deposition of silicon-based dielectrics for semiconductor manufacturing: current status and future outlook, J. Vac. Sci. Technol. A. 37 (2019) 060904, , https://doi.org/10.1116/1.5113631.

[22] J. Han, Y.J. Yin, D. Han, L.Z. Dong, Improved PECVD SixNy film as a mask layer for deep wet etching of the silicon, Mater. Res. Express (2017) 4, https://doi.org/10.1088/2053-1591/aa8782.

[23] K. Ohdaira, T.T. Cham, H. Matsumura, Passivation of textured crystalline silicon surfaces by catalytic CVD silicon nitride films and catalytic phosphorus doping, Jpn. J. Appl. Phys (2017) 56, https://doi.org/10.7567/JJAP.56.102301.

[24] T.S. Stokkan, H. Haug, C.K. Tang, E.S. Marstein, J. Gran, Enhanced surface passivation of predictable quantum efficient detectors by silicon nitride and silicon oxynitride/silicon nitride stack, J. Appl. Phys (2018) 124, https://doi.org/10.1063/1.5054696.

[25] B. Arkles, Y. Pan, F. Jove, N-alkyl substituted cyclic and oligomeric perhydridosilazanes and silicon nitride films formed therefrom, Eur. Patent 3 (2019) 274,354 B1.

[26] B. Arkles, Silicon Nitride from Organosilazane Cyclic and Linear Prepolymers, ECS J. Accel. Br. Commun 133 (1986) 232–234.

[27] H.-.Y. Shih, M.-.C. Lin, L.-.Y. Chen, M.-.J. Chen, Uniform {GaN} thin films grown on (100) silicon by remote plasma atomic layer deposition, Nanotechnology 26 (2014) 14002, https://doi.org/10.1088/0957-4484/26/1/014002.

[28] P. Motamedi, K. Cadien, Structural and optical characterization of low-temperature ALD crystalline AlN, J, Cryst. Growth. 421 (2015) 45–52, https://doi.org/10.1016/j.jcrysgro.2015.04.009.

[29] J.M. Park, S.J. Jang, S.I. Lee, W.J. Lee, Novel cyclosilazane-type silicon precursor and two-step plasma for plasma-enhanced atomic layer deposition of silicon nitride, ACS Appl. Mater. Interfaces 10 (2018) 9155–9163, https://doi.org/10.1021/acsami.7b19741.

[30] H.S. Kim, X. Meng, S.J. Kim, A.T. Lucero, L. Cheng, Y.C. Byun, J.S. Lee, S.M. Hwang, A.L.N. Kondusamy, R.M. Wallace, G. Goodman, A.S. Wan, M. Telgenhoff, B.K. Hwang, J. Kim, Investigation of the physical properties of plasma enhanced atomic layer deposited silicon nitride as etch stopper, ACS Appl. Mater. Interfaces 10 (2018) 44825–44833, https://doi.org/10.1021/acsami.8b15291.